SPE 121195

Enhanced Mass Transfer of CO_2 into Water: Experiment and Modeling

Rouhi Farajzadeh[1], Pacelli L.J. Zitha[1,2] and Hans Bruining[2]
[1] SPE and Shell International E&P, Rijswijk, The Netherlands
[2] SPE and Delft University of Technology, The Netherlands

This paper was prepared for presentation at the 2009 SPE EUROPEC/EAGE Annual Conference and Exhibition held in Amsterdam, The Netherlands, 8–11 June 2009.

Abstract

Global warming has increased interest in quantification of the dissolution of CO_2 in (sub)-surface water. CO_2 is present above the surface water. Dissolution of CO_2 into water (or oil) causes a density increase, with respect to pure water (or oil). This density effect causes natural convection, which enhances the mass transfer rate across the interface. This article describes a series of experiments performed in a cylindrical PVT-cell at a pressure range of p_i=*10-50 bar*, where a fixed volume of CO_2 gas was brought into contact with a column of distilled water. The results show that the mass transfer rate across the interface is much faster than predicted by Fickian diffusion. This mass transfer rate increases with increasing initial gas pressure and in the long term it is controlled by diffusion.

A theoretical interpretation of the observed effects has been proposed, based on diffusion and natural convection phenomena. The CO_2 concentration at the interface is estimated from the gas pressure using Henry's solubility law, in which the coefficient varies with both pressure and temperature. Good agreement between the experiments and the theoretical results has been obtained.

1. INTRODUCTION

Carbon Dioxide (CO_2) is one of the major greenhouse gases blamed for causing global warming [1]. To reduce the concentration of CO_2 in the atmosphere, geological storage of CO_2 is considered [2-4]. When CO_2 is injected into the saline aquifers, the brine will eventually be overlaid by CO_2 due to the buoyancy effects. Then, CO_2 dissolves into the brine by molecular diffusion. The density of the water-CO_2 solution exceeds the density of pure water and increases with increasing CO_2 concentration [5]. This can lead to natural convection effects [5,6]. Therefore, the quantification of CO_2 dissolution in water is important in predicting the potential and long-term behavior of CO_2 in aquifers.

Unfortunately there are only few experimental data in the literature, involving mass transfer between water and CO_2 under conditions of natural convection. Lindenberg and Wessel-Berg [7] were among the first to point out the importance of natural convection for sequestration of CO_2 in aquifers. Yang and Gu [8] performed experiments in bulk where a column of CO_2 at high pressure was in contact with water. A modified diffusion equation with an effective diffusivity was used to describe the mass-transfer process of CO_2 into the brine. A good agreement between the experiments and the model was observed by choosing effective diffusion coefficients two orders of magnitude larger than the molecular diffusivity of CO_2 into water. However, the authors pointed out that the accurate modeling of the experiments should consider natural convection effects. Farajzadeh et al. [9,10] reported experimental results for the same system, in a slightly different geometry, showing initially enhanced mass transfer and subsequently a classical diffusion behavior for long times. A physical model based on the Fick's second law and Henry's law was used to interpret the experimental data. However, it was found that the mass transfer process cannot be modeled with a modified Fick's second law with a single effective diffusion coefficient for the CO_2-water system at high pressures. Nevertheless, the initial stages and later stages of the experiments can be modeled individually with the described model and two effective diffusion coefficients could be obtained from the experimental data. Arendt et al. [11] applied a Schlieren method and a three-mode magnetic suspension balance connected to an optical cell to analyze the mass transfer of the CO_2-water system up to *360 bar*. A good agreement between their model (linear superposition of *free convection* and Marangoni convection) and the experiment was obtained. The addition of surfactant suppressed the Marangoni convection in their experiments, while in the experiments of ref. [9] addition of surfactant did not have a significant effect on the transfer rate of CO_2. Nghiem et al. [12] gave a field example to show that natural convection is an important mechanism in CO_2 sequestration in aquifers. A similar mass transfer enhancement was observed for the mass transfer between a gaseous CO_2 rich phase with two hydrocarbons (n-decane and n-hexadecane) [9,10] due to the fact that

CO_2 increases the hydrocarbon density [13]. The effect is less significant for n-hexadecane due to its higher viscosity. This has implications for oil recovery.

The theoretical description of temperature driven natural convection flow uses Navier-Stokes equation and can be found in classical books on fluid mechanics [14,15]. Several numerical approaches have been proposed to solve the governing Navier-Stokes and continuity equations. Guçeri and Farouk [16] derived a numerical model for steady state natural (turbulent) convection in various geometries. By the symmetry of the geometries considered they can use the stream function-vorticity approach. From the mathematical point of view these geometries allow a 2D description. Patankar [17] proposed a semi-implicit numerical method, which can also be used to (non-steady) 3D problems. Bairi [18] used Patankar's method to study the transient natural convection in a 2D vertical cylinder. Increasingly, the Finite Element Method (FEM), which was originally developed for solid mechanics calculations, is being applied in this area. This method facilitates the modeling of the problem in complex geometries with irregularities [19-21]. Moreover, non-uniform meshes can easily be used in this method which allow for the resolution of flow details in the regions of interest.

The purpose of this paper is two fold. The first purpose is to add experimental data to the currently small database in the literature. The second goal is to develop a model that can fully describe the experiments without having to introduce (semi) empirical parameters. It turns out that this is possible by considering density-driven natural convection phenomenon. Therefore, this paper focuses on describing the phenomena, both experimentally and numerically, when a CO_2 rich gaseous phase is on top of a water layer. Section 2 describes the geometry of the system and the physical model to study the natural convection in a vertical cylinder. Section 3 explains the experimental setup, i.e., a vertical cylindrical PVT cell and the experimental procedures. Section 4 presents the experimental results and compares it with the numerical computations. Finally we draw the main conclusions of this study.

2. THEORETICAL MODEL

2.1. Formulation

There can only be mechanical equilibrium in a fluid in a gravitational field if the concentration of CO_2 inside the liquid only varies in the vertical coordinate, i.e., $c = c(z)$. However if the concentration gradient exceeds a certain value mechanical equilibrium in the fluid will be impossible [15]. The instability will initiate a convection current. This process will develop into natural convection throughout the entire fluid and the concentration becomes dependent on the radial coordinate as well. The driving force for natural convection is due to the fact that dissolution of CO_2 into water causes a density increase. Consequently fresh (no-CO_2 containing) water moves to the interface and CO_2 containing water moves downwards, accelerating the diffusion process, and hence the mass transfer rate. The mixing of the water finally leads to a constant CO_2 concentration in the water.

We try to formulate such motions inside the water when it is brought into contact with a CO_2 rich gaseous phase in the geometry depicted in Fig. 1. The cylindrical vessel with radius R consists of an upper column filled with gaseous CO_2 and a lower column filled with a stagnant water layer. We disregard both water evaporation (the contribution of water vapor to the gas pressure is *4.25 kPa* at *T=30°C* which is negligible compared to the experimental pressure drop [22]) and water swelling due to CO_2 dissolution. Consequently we assume that the boundary remains fixed. This assumption arises from the fact that the volume change of CO_2-water binary mixture is very small at the range of our experimental pressures. It is assumed that capillary effects are absent and therefore the interface is flat. The gas transfer at the upper cell (gas phase) is largely governed by mechanical equilibrium, but can be adequately described by Fick's law with a high constant diffusion coefficient. CO_2 will be removed at the CO_2-water interface. This decreases the concentration of CO_2 at the interface and increases concentration of water. However, water concentration cannot deviate too far from equilibrium, as otherwise water will condense. Consequently, even with slow diffusion rates (of the order of $10^{-5}P_{atm}/P_{exp}$ m^2/s) the concentration of CO_2 will not significantly deviate from its equilibrium value at the time scale of the experiment. The CO_2 concentration at the liquid surface is related to the gas pressure by assuming instantaneous thermodynamic equilibrium at the interface by applying Henry's law. The characteristic time for conversion of $CO_2+H_2O \rightarrow H_2CO_3$ is *1/0.039 ~ 25* seconds, which is much smaller than the experimental times. Moreover, only very small amount of CO_2 is converted to H_2CO_3. The dissociation into HCO_3^- and CO_3^{2-} is negligible and therefore the rates of their formation can be ignored. We assert that the transfer of gas through the CO_2-water interface can be described as an unsteady-state diffusion process, i.e., by Fick's law.

The conservation laws for the two components (CO_2 and water) and momentum in the liquid are the governing equations to describe the diffusion and natural convection; the analogy between mass and heat transfer allows us to use the equations in Refs. [14-16]. Only a laminar regime is expected, as the Rayleigh number is of the order of 10^6. The density difference is the driving force for natural convection and consequently it cannot be considered constant. However, we use the Boussinesq approximation, which considers density variations only when they contribute directly to the fluid motion. Moreover we assume that there is a linear relationship between density change and concentration

$$\Delta\rho = \beta_c \rho_i \Delta c \,. \tag{1}$$

Symbols are defined at the end of the paper. The characteristic behavior of the density of a CO_2-water solution on pressure and temperature can be found in Ref. [5]. For the pressures and temperatures of interest the data are presented in Fig. 2. The time dependent governing equations for a 2D diffusion and natural convection system can be written in radial coordinates (see Fig. 1 for a schematic of the setup and the area of interest), as described below.

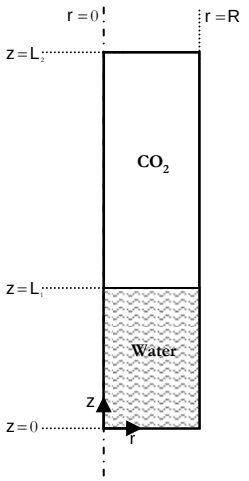

Fig. 1: Schematic outlay of the process: The total length of the tube is L, the height of water is L_1. There is no gas flowing out at the end of the tube. The gas-liquid interface is fixed. The liquid concentration at the interface is related to the gas pressure through Henry's Law and changes with time.

2.2. Governing equations

2.2.1. Liquid phase

(a) Continuity equation

$$div\ \mathbf{v} = 0\ . \tag{2}$$

(b) Conservation of momentum

$$\frac{\partial \mathbf{v}}{\partial t} + \left(\mathbf{v}.\mathbf{grad}\right)\mathbf{v} = -\frac{1}{\rho}\mathbf{grad}p + \nu\Delta\mathbf{v} - \beta_c \mathbf{g}\Delta c \quad . \tag{3}$$

(c) Concentration equation

$$\frac{\partial c}{\partial t} + \mathbf{v}.\mathbf{grad}c = D\Delta c \quad . \tag{4}$$

2.2.2. Gas phase

$$\frac{\partial c_g}{\partial t} = D_g \Delta c_g \quad . \tag{5}$$

One important dimensionless number in fluid dynamics is the Rayleigh number, which is dependent on the fluid properties and geometry of the system (characteristic length of the system) with the following relation

$$Ra = \frac{\beta_c g \Delta c R^3}{\nu D} = \frac{\Delta\rho g R^3}{\rho_i \nu D} \quad , \tag{6}$$

where, we use Eq. (1) to replace β_c. Equation (6) states that the magnitude of Rayleigh number depends on the geometry of the experimental setup, in this case the radius of the tube, and properties of the fluid. These properties include the diffusion coefficient of gas into water, viscosity of water and its density change due to gas dissolution. As mentioned before in our case this density change is a strong function of the CO_2 concentration, i.e., the initial pressure of the CO_2. This means that a high Rayleigh number is due to a large radius of the tube or a high initial pressure or the combination of both parameters.

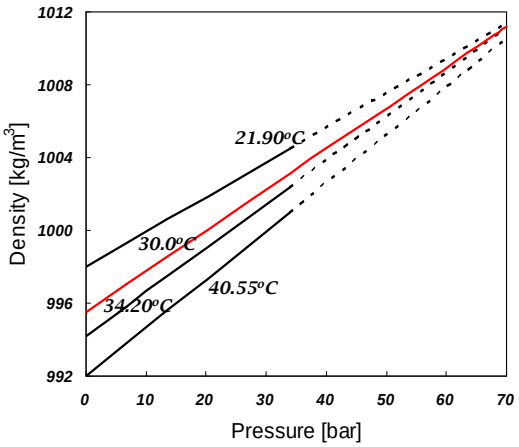

Fig. 2: Density of water as a function CO_2 concentration (equilibrium pressure). The dashed lines are extrapolated from the solid lines reproduced from the data in ref. [5].

2.3. Boundary and initial conditions

2.3.1. Liquid phase

Initially the liquid is at rest and there is no CO_2 dissolved in the water, i.e.,

$$\mathrm{v} = c = 0 \ \text{ at } \ t = 0 \quad . \tag{7}$$

The boundary conditions of the problem are

$$\begin{aligned} &\partial_r c = 0 \ \ at \ r = 0, \\ &\mathrm{v} = 0, \ \partial_r c = 0 \ \ at \ r = R, \\ &\mathrm{v} = 0, \ \partial_z c = 0 \ at \ z = 0, \\ &c = p_g / k_H = \left(Z_g R_B T / k_H \right) c_g \ \ at \ z = L_1. \end{aligned} \tag{8}$$

2.3.2. Gas phase

Initially the gas part is filled with gas at pressure p_i and therefore the molar gas concentration reads,

$$c_g \left(x, t = 0 \right) = \frac{p_i}{Z_g R_B T} \quad . \tag{9}$$

The boundary conditions are

$$\begin{aligned} &\partial_r c_g = 0 \ \ at \ r = 0, \\ &\partial_r c_g = 0 \ \ at \ r = R, \\ &J_z = -D \partial_z c_g \ \ at \ z = L_1, \\ &\partial_z c_g = 0 \ at \ z = L_2. \end{aligned} \tag{10}$$

2.4. Henry's law (CO_2 solubility) at the interface

The solubility of CO_2 in water can be expressed by using Henry's law as:

$$x_{CO_2(aq)} = \frac{f_{CO_2(P,T)} y \gamma_y}{k^*_{H(P,T)} \gamma_{CO_2(aq)}} \quad , \tag{11}$$

where, x_{CO2} and y are the mole fractions of CO_2 in liquid and gas phases, respectively, k^*_H is Henry's constant [in Pa] that is dependent on pressure and temperature, γ_{CO_2} is the asymmetric (Henry's law) activity coefficient of aqueous CO_2 such that $\gamma_{CO_2(aq)} \to 1$ as $x_{CO_2(aq)} \to 0$ and γ_y is the symmetric (Raoult's law) activity coefficient of CO_2 in the non-aqueous phase,

such that $\gamma_y \to 1$ as $y \to 1$ and f_{CO_2} is the fugacity of pure CO_2 at specified P-T conditions. Henry's coefficient, k_H^*, can be calculated from the virial-like equation of state of Akinfiev and Diamond [23]

$$\ln\left(k_H^*\right) = \left(1-\xi\right)\ln f_w + \xi \ln\left(\frac{R_B T}{M_w}\rho_w\right) + 2\rho_w\left[a + b\left(\frac{1000}{T}\right)^{0.5}\right]. \quad (12)$$

Diamond and Akinfiev [24] developed a thermodynamic model that reproduces 362 published experimental solubility data with a precision of better than 2% over the entire *P-T-x* considered. We used their model to calculate Henry's coefficient (the model is available as a computer code at www.geo.unibe.ch/diamond). The dependency of Henry's coefficient, k_H (in Pa/mol/m^3), on pressure at a constant experimental temperature of $T=30^oC$ is shown in Fig. 3. Henry's coefficient varies slightly with pressure at a constant temperature.

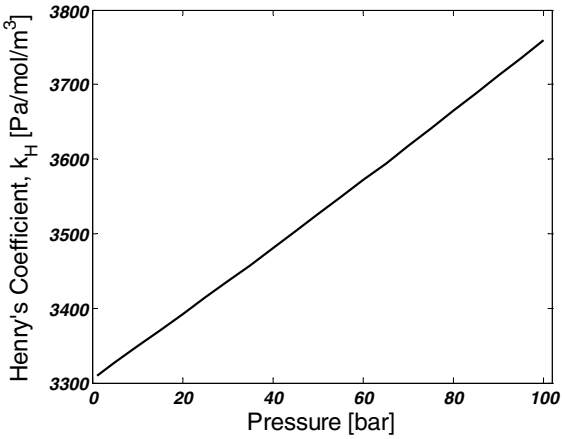

Fig. 3: Henry's coefficient, k_H, as a function of pressure calculated using Eq. (12) at a constant temperature of T=30°C.

2.5. Numerical Scheme and solution procedure

The equations were solved numerically using the Finite Element Method software package, Comsol multiphysics. COMSOL is a software package that can solve various coupled engineering and physics problems, e.g., here a combination of Navier-Stokes, convection-diffusion and diffusion equation in the geometry depicted in Fig. 1.

3. EXPERIMENTAL

3.1. Materials

The gas used to carry out the experiments was 99.98% pure carbon dioxide. CO_2 is highly soluble in water [25]. The diffusion coefficient of CO_2 in water is $(D=1.97\pm0.10)\times10^{-9}m^2/s$ [26]. Nitrogen (N_2) was used to detect possible leakages in the setup. Water with $pH=6.8\pm0.1$ was used in the experiments.

3.2. Set-up and procedure

Figure 4 shows the schematic of the experimental set-up. It consists of two stainless steel vessels, the measurement vessel with inner diameter of $D_1=30mm$ and the gas storage vessel with an inner diameter of $D_2=40mm$. The length of both vessels is 10cm. The vessels are sealed and kept at constant temperature of $T=30\pm0.1^oC$ in an oven. Characteristic time at which temperature equilibrates (~ *1500sec*) has been determined by numerical simulation, where the vessel was subjected to conductive and radiation heat loss. To ensure that the vessels remain in a fixed position they were attached to a board. Before starting the measurements a leakage test was performed with nitrogen. A valve at the bottom of the measurement cell was used to fill the vessel with double distilled water up to the desired height ($L_1=43mm$) using a pump with a known flow rate. A waiting time of approximately 1 hour was then respected, in order to let the liquid come into thermal equilibrium with the oven. CO_2 was slowly injected into the measurement vessel from the storage vessel. The gas pressure is measured with two calibrated pressure gauges, which are connected to the top of the vessels. When the CO_2 pressure reached the desired value, the valve connecting the vessel containing the water was closed and the cell was isolated. This was the starting time of the experiment. The gas pressure was recorded every *100* seconds in a computer.

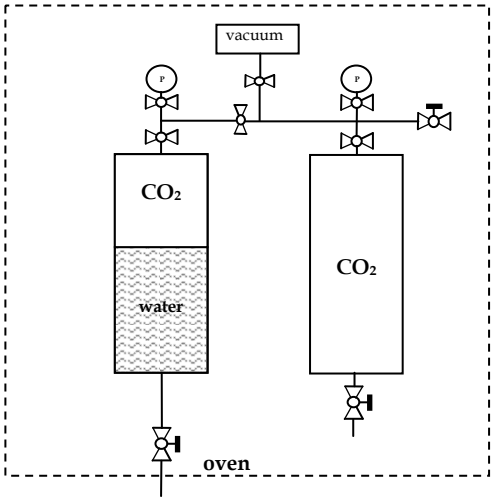

Fig. 4: Schematic of the set-up: The set-up consists of two steel vessels, a storage vessel (right) and a measurement vessel (left). The gas at pressure pi is injected from the right vessel to the left vessel. Mass transfer occurs through the interface in the left vessel. The set-up is held in an oven at a constant temperature. The pressure of the gas at the top part is monitored by a pressure transducer.

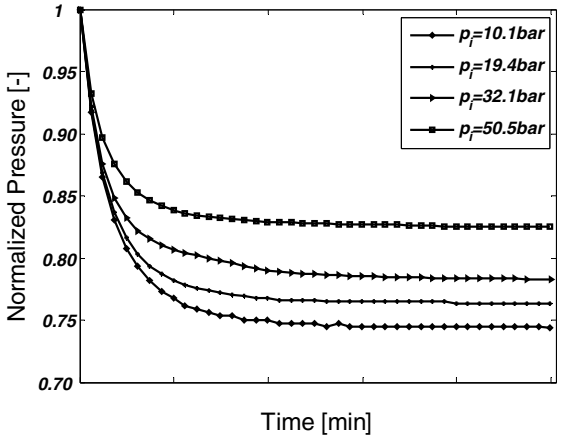

Fig. 5: Pressure history of the experiments with different initial pressures. The pressure decline indicates the transfer of CO_2 into water. Initially the curves are steeper showing the significance of natural convection.

4. RESULTS & DISCUSSION

4.1. Experimental observations

Figure 5 shows the normalized CO_2 pressure versus time during the experiments with different initial pressures. The gas pressure declines significantly at the initial stages of the experiment, i.e., it has a steep slope at the early times of the experiment. However, the slope of the curve becomes less steep with time, meaning that the mass transfer rate decreases with time. The time needed for an over-pressurized gas to reach equilibrium with the liquid below can be calculated using Fick's second law. However, in our experiments the measured mass-transfer rate over the interface turned out to be substantially larger than predicted using Fick's second law (see the dashed lines in Figs. 11-14). An interpretation in terms of *two effective diffusion coefficients* has been presented in Ref. [9]. The effective diffusion coefficient for the early stages of the experiments is two orders of magnitude higher than the molecular diffusivity of the CO_2 into water, indicating the presence of natural convection. The effect of natural convection increases as the initial pressure of the experiments increases. Nevertheless in all experiments the influence of the convection decreases as time elapses regardless of the initial pressure of the experiment.

4.2. CO_2 concentration inside the liquid

The general trend of the concentration profiles for all experiments is similar and therefore only the curves of the experiment with p_i*=10.1 bar* will be presented. Nonetheless, the explanation holds for all experiments. Figure 6 shows the evolution of CO_2 concentration inside the water with time. The maximum and minimum concentrations are given below each image. These maximum (red) and minimum (blue) concentration values are different in each panel. This procedure allows using the full color span for displaying the results. When analyzing this profile, it is observed that as soon as CO_2 is put above the water, it starts to dissolve. The CO_2 concentration is higher near the center of the vessel. This increases the density of the

liquid near the center, which induces an anti-clockwise vortex in the vessel. The CO_2 concentration decreases at the interface (and near the interface) as the pressure in the gas chamber decreases while CO_2 is transferred far into the liquid. After about *30* minutes CO_2 reaches the bottom of the vessel. At this time the fluid has its maximum velocity (see Fig. 7). With a simple scaling analysis it is possible to evaluate the significance of natural convection. The time scale for CO_2 diffusion through a water layer with thickness of L_1=*43mm* at our experimental condition is $\sim L_1^2/D \approx 9.24\times10^5 sec \approx 256hr >> 30$ *minutes*. As time elapses, the difference between the minimum and maximum values of the concentration becomes less, i.e., the distribution of CO_2 becomes more uniform in the liquid. This implies that convection effect die out with time.

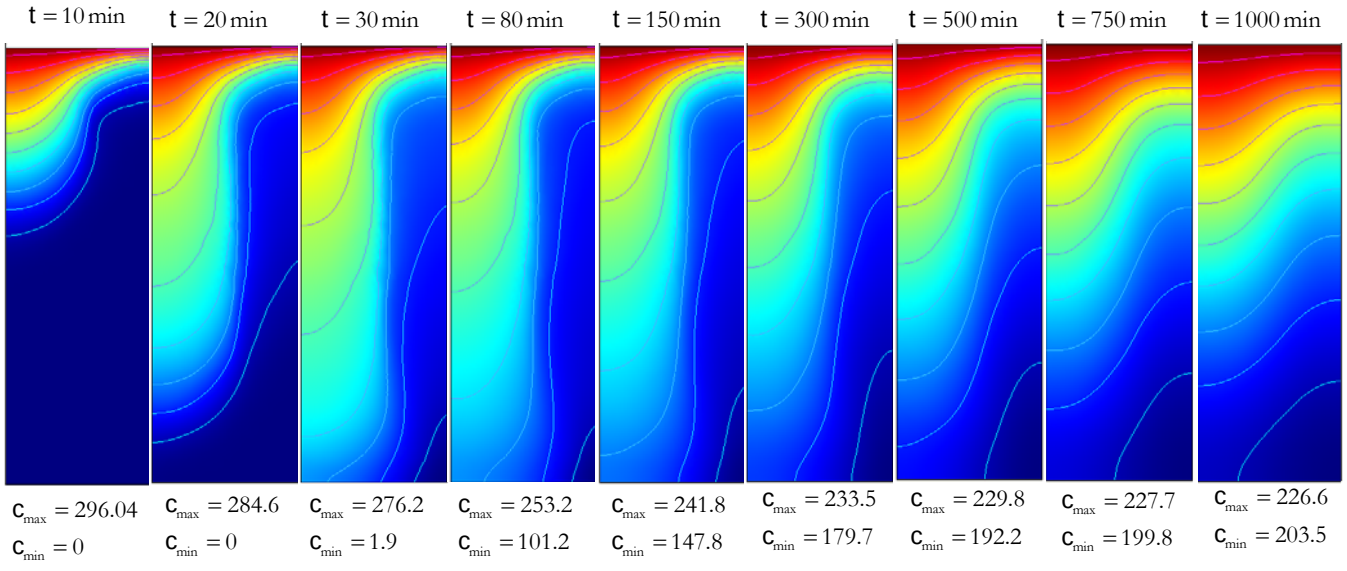

Fig. 6: Evolution of CO_2 concentration profiles inside water with time at an initial pressure of p_i=*10.1* bar. The maximum (red) and minimum (blue) concentration values are different in each panel. The concentration values are expressed in [mol/m^3].

4.3. Velocity profiles

Figure 7 presents the calculated vertical velocity, v_z, at different vertical positions as a function of the vessel radius for the experiment with the initial pressure of p_i=*10.1 bar*. In accordance with the concentration profile, the flow is much faster in the center, obviously to ensure (water) mass conservation in a horizontal cross section. In the entire volume of the vessel the ascending fluid flow has a low velocity close to the wall, where it approaches zero corresponding to the adherence of the fluid. The vertical velocity increases as fluid moves down in the region *43<z<33 mm*. From *z=33mm* downwards the fluid starts to slow down again until it stops at the bottom of the vessel (z=0). In other words the flow is slower at the upper part close to the CO_2-water interface. A similar velocity pattern was numerically observed for a cylindrical cavity when its upper face was cooled by themoelectrical Peltier effect following an exponential law [18]. It appears from the simulation results that at *z=33mm* there is no flow in the radial direction (see Fig. 8). The radial velocity is one order of magnitude smaller than the vertical velocity and it has different signs below and above *z=33mm*. This means that the vertical flow is mainly responsible for the enhancement of transfer rate of CO_2 into water. The velocity change with time is shown in Fig. 9 at a fixed position of *z=30 mm*. Initially the liquid is at rest. When CO_2 in brought in contact with the liquid it starts to move. The liquid velocity increases until the CO_2 front reaches the bottom of the vessel at t~30 minutes. After that the fluid velocity decreases as more CO_2 is dissolved in the water with time. Note that at the end of our experiment the liquid velocity is very low but not zero. The fluid motion stops after about *3000* minutes when the water is fully saturated with CO_2. As can be seen from Fig. 10 the liquid velocity increases as the initial pressure of the experiment (or the Rayleigh number) increases. Obviously, the relation is not linear. The pressure decline becomes faster as the Rayleigh number increases, i.e., the time to reach the equilibrium state for a constant volume of water decreases with increasing Rayleigh number, a result which can also be concluded from Fig. 5.

4.4. Pressure decline

As already mentioned CO_2 was injected from the storage vessel to the measurement vessel that was initially filled with water at atmosphere pressure. The sudden opening of the valve between the two vessels causes disturbances, which may hamper a clear definition of the initial conditions. All the same adiabatic compression of CO_2 temporarily increases the temperature of the vessel [27]. As a result the system requires a short time to equilibrate. This effect is more significant at higher pressure as larger mass of CO_2 is injected to the system. Our system measures pressures with 100 second intervals; therefore, we ignored the first two data points. This time is equivalent to the time at which CO_2 reaches equilibrium in the storage vessel (the

pressure remains constant). In ref. [8] the authors ignored first *180* seconds of their experiments due to a similar effect.
Figures 11-14 plot the pressure history for the experiments with the initial pressures of p_i*=10.1, 19.4, 32.1 and 50.5 bar* respectively. These pressures are well below the critical pressure of CO_2. The experimental data are compared with the theory described in Section 2 with and without taking into account natural convection effects. In all cases the pressure decline rate is much larger than predicted by a Fickian diffusion process. For the computations values of β_c, k_H and Z_g are required. Note that by choosing β_c=0 in the simulation, diffusion will be the only transport mechanism and therefore the results of model agree well with the analytical solution obtained in Ref. [9]. In the case of natural convection, the density differences are read from Fig. 2 and then the concentration dependent β_c is calculated for the conditions of each experiment using Eq. (1). Henry's coefficient, k_H, is obtained from Fig. 3. The compressibility factor, Z_g, is calculated using the Span-Wagner EoS [28] for all pressures at the experimental temperature ($T=30^oC$). For all of the experiments the match between the experimental data and the theory is within the experimental error (solid lines). To obtain the solid lines, the molecular diffusion coefficient of CO_2 ($D=2.0\times10^{-9}$ m^2/s) was used in the model. It is also possible to fit the experimental data by choosing *effective diffusion coefficients* and switching off the convection currents (dotted lines), similar to the models explained in refs. [8,9]. Such models are not physically justified, because comparing the values reported in ref. [9] for p_i*=10.1 and 19.4 bar* and the values obtained from our simulations reveal that the magnitude of the diffusion coefficient depends on the geometry of the system (in this case radius and aspect ratio). Moreover, these models fail in accurately explaining the later stages of the experiments, because allowing an effective diffusion coefficient two orders of magnitude larger than molecular diffusivity of CO_2 results in equilibration times that are much shorter than the experiments [see Figs. 11-14]. In ref. [8] the authors simulate experiments with duration of only one hour. The extracted effective diffusion coefficients increase with increasing initial pressure and they are in good agreement with the values reported in ref. [8].

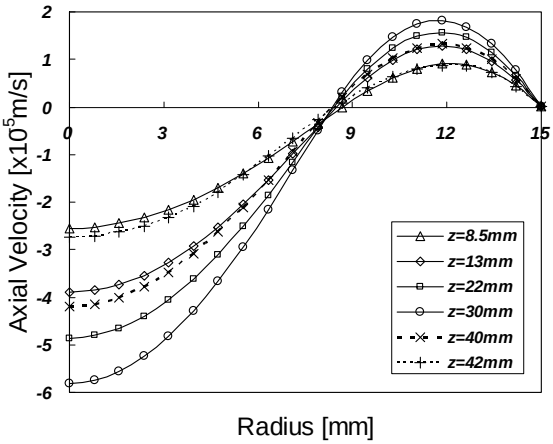

Fig. 7: Axial velocity, v_z, at different positions at *t=60min* for the experiment with an initial pressure of p_i*=10.1 bar*.

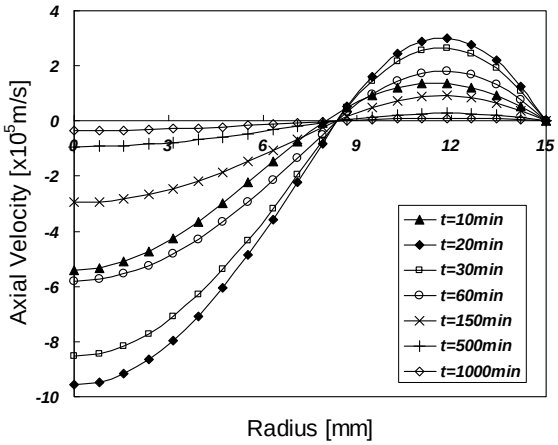

Fig. 9: Axial velocity, v_z, at different times at *z=30mm* for the experiment with an initial pressure of p_i*=10.1 bar*.

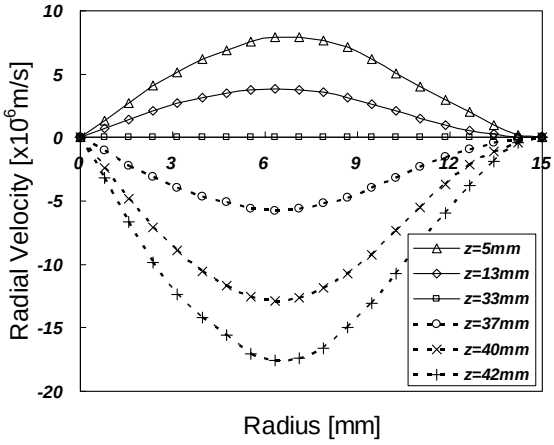

Fig. 8: Radial velocity, v_r, at different positions at time *t=60min* for the experiment with an initial pressure of p_i*=10.1 bar*.

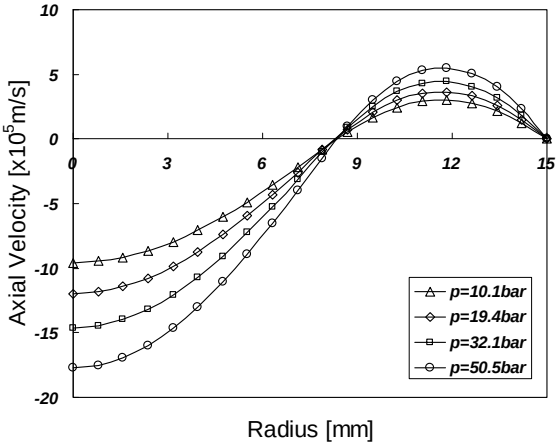

Fig. 10: The calculated axial velocity, v_z, at *z=30mm* and *t=20min* for the experiments with different initial ressures

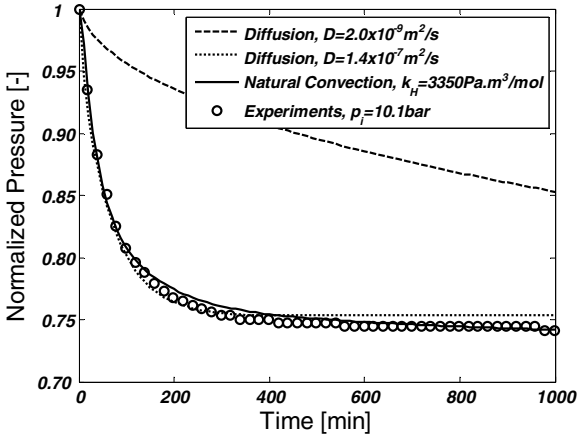

Fig. 11: Comparison between the measured pressure data and the numerical model for p_i=10.1 bar, T=30 ^oC, k_H=3350 *Pa.m^3/mol* and D=2.0×10^{-9} *m^2/sec.* The dotted line is obtained with an effective diffusion coefficient of *D=1.40×10^{-7} m^2/sec.*

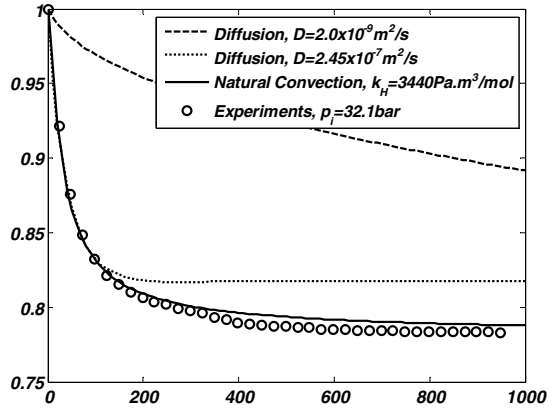

Fig. 13: Comparison between the measured pressure data and the numerical model for *p_i=32.1 bar, T=30^oC, k_H=3440 Pa.m^3/mol and D=2.0×10^{-9} m^2/sec*. The dotted line is obtained with an effective diffusion coefficient of *D=2.45×10^{-7} m^2/sec.*

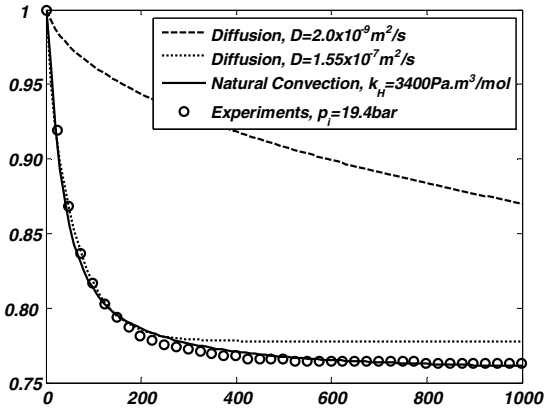

Fig. 12: Comparison between the measured pressure data and the numerical model for p_i=19.4 bar, *T*=30^oC, k_H=3400 *Pa.m^3/mol* and *D*=2.0×10^{-9} *m^2/sec.* The dotted line is obtained with an effective diffusion coefficient of *D=1.55×10^{-7} m^2/sec.*

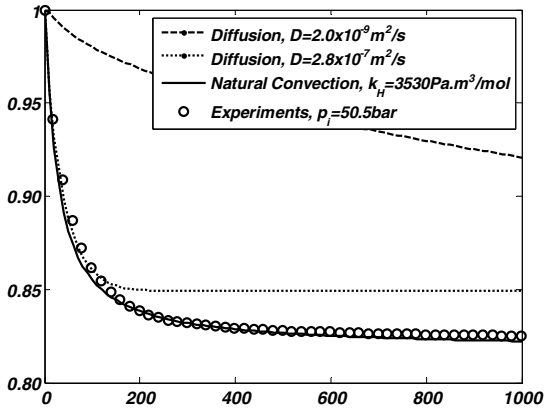

Fig. 14: Comparison between the measured pressure data and the numerical model for *p_i=50.5 bar, T=30^oC, k_H=3530 Pa.m^3/mol and D=2.0×10^{-9} m^2/sec*. The dotted line is obtained with an effective diffusion coefficient of *D=2.80×10^{-7} m^2/sec.*

5. CONCLUSIONS

- We confirmed that mass transfer rates can be measured in a relatively simple PVT cell, following pressure history of the gas phase by extending our experimental data base to pressure range of 10-50 bar.
- A physical model based on density-driven natural convection and diffusion has been formulated. The model uses a number of simplifying assumptions, e.g., that Henry's law is applicable at the interface.
- The Finite Volume Method (FVM) was used to solve the model equations numerically. The validity of the model was confirmed by comparing to benchmark solutions. We used these results to validate a Finite Element Model (FEM) using COMSOL. The advantage of using FEM is that local grid refinement is easier.
- According to the simulations the velocity increases until it reaches a maximum and then diminishes gradually as natural convection effect become less important. The maximum velocity corresponds to the time in which CO_2 front reaches the bottom of the vessel.
- There is a strong correlation between the fluid velocity and the concentration profile with the experimental pressure decline rates. The pressure history obtained from the numerical model agrees well with the experimental data within experimental error. The matching does not use any fitting parameters.

6. ACKNOWLEDGEMENTS

This research was carried out as part of a project funded by Delft Earth Research. We thank the technicians of the Dietz laboratory of our faculty, especially H. van der Meulen and H. van Asten. We thank Prof. A. Firoozabadi and Dr. S. Rudolph for useful suggestions.

7. NOMENCLATURE

c	*Concentration [mol/m^3]*
c_p	*Heat capacity [J/K/m^3]*
D	*Diffusion coefficient [m^2/s]*
f	*Fugacity [Pa]*
g	*acceleration due to gravity [m/s^2]*
k_H	*Henry's constant*
L	*Length of the tube [m]*
M	*Molecular weight [kg/mol]*
p	*Pressure [Pa]*
r	*Distance from center of the tube [m]*
R	*Radius of the tube [m]*
Ra	*Rayleigh number [-]*
T	*Temperature [K, ^{o}C]*
t	*Time [sec]*
v	*Velocity [m/s]*
z	*Distance from the bottom of the tube [m]*
Zg	*Gas compressibility factor [-]*

Greek symbols

ρ	*Density of the fluid [kg / m^3]*
β_c	*Volumetric expansion coefficient [m^3/mol]*
ξ, a, b	*Empirical fitting parameters*
μ	*Viscosity of the fluid [kg / m − sec]*
ν	*Kinematic viscosity [m^2/s]*

Subscripts

0	*Reference value of the quantity*
g	*Gas*
i	*Initial value of the quantity*
w	*Water*
r	*Quantity in* r*-direction*
Z	*Quantity in* z*-direction*

8. REFERENCES

1. IPCC special report on Carbon Dioxide capture and storage, Edited by B. Metrz, O. Davidson, H. de Coninck, M. Loos, L. Meyer, *Cambridge University Press* (2005).
2. K. Pruess and J. Garcia, Multiphase flow dynamics during CO_2 disposal into saline aquifers, *Environ. Geol.,* **2002,** 42, 282.
3. R.G. Bruant, A.J. Guswa, M.A. Celia, C.A. Peters, Safe storage of CO_2 in deep saline aquifers, *Environmental Science and Technology*, June 1, **2002,** 241A-245A.
4. A. Naderi Beni, M. Kühn, R. Meyer, C. Clauser, Geological sequestration of CO_2 in North Rhine Westphalia (Germany), *Proceedings of the Sino-German Workshop, Goslar*, Germany, 17-20 September 2007.
5. L. Gmelin, in: *Gmelin Handbuch der anorganischen Chemie*, 8. Auflage. Kohlenstoff, Teil C3, Verbindungen. ISBN 3-527-81419-1 (1973).
6. R. Farajzadeh, H. Salimi, P.L.J. Zitha, J. Bruining, Numerical simulation of density-driven natural convection with application for CO_2 injection projects, *Int. J. Heat and Mass Transfer,* **2007**, 50, 5054.
7. E. Lindenberg and D. Wessel-Berg, Vertical convection in an aquifer column under a gas cap of CO_2, *Energy Convers. Mgmt*, **1997,** Vol. 38, Suppl., S229-S234.
8. C. Yang and Y. Gu, Accelerated Mass Transfer of CO_2 in Reservoir Brine Due to Density-Driven Natural Convection at High Pressures and Elevated Temperatures, *Ind. Eng. Chem. Res.,* **2006,** 45 (8), 2430.

9. R. Farajzadeh, A. Barati, H.A. Delil, J. Bruining, P.L.J. Zitha, Mass Transfer of CO_2 into Water and Surfactant Solutions, *Petrol. Sci. and Technol.,* **2007,** 25, 1493.
10. R. Farajzadeh, H.A. Delil, P.L.J. Zitha, J. Bruining, Enhanced Mass Transfer of CO_2 into Water and Oil by Natural Convection, *SPE 107380*, EUROPEC London, The UK (2007).
11. B. Arendt, D. Dittmar, R. Eggers, Interaction of interfacial convection and mass transfer effects in the system CO_2–water, *Int. J. Heat and Mass Trans.*, **2004,** 47, Issues 17-18, 3649.
12. L. Nghiem, P. Sammon, J. Grabensetter and H. Okhuma, Modeling CO_2 Storage in Aquifers with a Fully-Coupled Geochemical EOS Compositional Simulator, In *SPE/DOE Fourteenth Symposium on Improved Oil Recovery, Tulsa, Oklahoma, U.S.A., SPE 89474* (2004).
13. S. Ashcroft and M. Ben Isa, Effect of dissolved gases on the densities of hydrocarbons, *J. Chem. Eng. Data*, **1997**, 42(6), 1244.
14. R.B. Bird, W.E. Stewart and E.N. Lightfoot, *Transport phenomena,* 2nd rev. ed., New York: Willey, (2007).
15. L.D. Landau and E.M. Lifshitz, *Fluid mechanics, Volume 6 of course of theoretical physics,* translated from Russian by Sykes J.B. and Reid W.H., pp. 212-218, 4th Edition, Pergamon Press (1975).
16. S. Guçeri and B. Farouk, *Numerical solutions in laminar and turbulent natural convection,* In: Natural convection, Fundamentals and applications, S. Kakac, W. Aung, R. Viskanta, Hemisphere publication, pp. 615-655 (1985).
17. S.V. Patankar and D.B. Spalding, A calculation procedure for heat, mass and momentum transfer in three dimensional parabolic flows, *Int. J. Heat Mass Transfer*, **1972**, 15, 1787.
18. A. Bairi, Transient natural 2D convection in a cylindrical cavity with the upper face cooled by thermoelectric Peltier effect following an exponential law, *Applied Thermal Engineering*, **2003,** 23, 431.
19. B.R. Becker and J.B. Drake, Finite element simulation of viscous incompressible flows, *Mathematical Modelling,* **1987,** 8, 245.
20. S. Ferreira, Transient natural convection cooling of a vertical circular cylinder, *Nuclear Engineering and Design,* **1974,** 31, 346.
21. B. Ramaswamy, Solution of the boussinesq equations by the finite element method, *Finite Element in Analysis and Design,* **1989,** 6, 319.
22. N.N. Greenwood and A. Earnshaw, *Chemistry of the elements*, 2nd Ed. Butterworth Heinemann, Oxford (1997).
23. N.N. Akinfiev and L.W. Diamond, Thermodynamic description of aqueous nonelectrolytes at infinite dilution over a wide range of state parameters, *Geochim. Cosmochim. Acta,* **2003,** 67, 613.
24. L.W. Diamond and N.N. Akinfiev, Solubility of CO2 in water from −1.5 to 100 °C and from 0.1 to 100 MPa: evaluation of literature data and thermodynamic modeling, *Fluid Phase Equilibria,* **2003,** 208, 265.
25. P.G.T. Fogg and W. Gerrard, Solubility of gases in liquids, Wiley, New York, 1991, pp 281-314.
26. Kh. Gertz and Hh. Loeschcke, Determination of diffusion coefficient of CO2 in the water with a conic tube, *Helv. Physiol. Pharmacol. Acta.*, **1954,** 12(4) C 72-4.
27. W.C. Edmister and B.I. Lee, *In: Applied Hydrocarbon Thermodynamics*, 2nd Ed., Gulf Publishing Company: Houston, TX, Vol1 (1984).
28. R. Span and W. Wagner, A New Equation of State for Carbon Dioxide Covering the Fluid Region from the Triple-Point Temperature to 1100 K at Pressures up to 800 MPa, *J. Phys. Chem. Ref. Data,* **1996**, 25 (6), 1509.